Néel temperature of stoichiometric La_2CuO_4

J. Saylor, L. Takacs, and C. Hohenemser
Department of Physics, Clark University, Worcester, Massachusetts 01610

J. I. Budnick
Department of Physics, University of Connecticut, Storrs, Connecticut 06268

B. Chamberland
Department of Chemistry, University of Connecticut, Storrs, Connecticut 06268
(Received 17 February 1989)

Following doping with ^{111}In in O_2 gas at 1273 K, samples of La_2CuO_{4+y} were subjected to vacuum anneals of varying lengths to adjust the oxygen content. Susceptibility studies show that vacuum anneals of ~ 13 h, starting at 1083 K and terminating at 873 K, consistently produce magnetic ordering at Néel temperature (T_N) = 317(3) K, the highest value yet published. Perturbed-angular-correlation (PAC) studies of the same samples, using the 171–245-keV $\gamma\gamma$ cascade of ^{111}Cd populated via the decay of ^{111}In, exhibit a combined magnetic-dipole–electric-quadrupole interaction. Analysis of this yields a magnetic hyperfine field and an electric-field-gradient asymmetry that follow the expected temperature dependence of the local magnetization and orthorhombic distortion, respectively. The samples have uniquely static and homogeneous hyperfine interactions with undetectable PAC line broadening. We argue that this implies a "defect-free" probe environment which we identify as stoichiometric with $y \cong 0$. Assuming that any residual defects are randomly distributed on oxygen lattice sites, we find $|y| \leq 0.016$.

I. INTRODUCTION

The phase diagram of La_2CuO_{4+y} plays a central role in the still evolving theories of high-temperature superconductivity. Its general structure, which involves orthorhombic and tetragonal lattices, as well as Néel, insulating, metallic, superconducting, and possible spin-glass phases, has been the object of much recent work.[1]

Particularly striking is the rapid decline of T_N with increasing oxygen and/or Sr content. For dilution of two-dimensional square-lattice antiferromagnets, such as $Rb_2Mn_{1-x}Mg_xF_4$ and $Rb_2Co_{1-x}Mg_xF_4$ the site percolation threshold is measured[2,3] and predicted[4,5] to be $x = 0.41$. For La_2CuO_{4+y} (Refs. 6 and 7) and $La_{2-x}Sr_xCuO_4$ (Refs. 8 and 9), on the other hand, the threshold in x and y occurs at about $\frac{1}{20}$ of the conventional percolation limit. This behavior is attributed to magnetic frustration arising from incompatibility of antiferromagnetic ordering in the Cu planes and ferromagnetic coupling induced via electron holes.[10–12] From the similarity of the phase diagrams,[8,13–16] Sr doping and increasing the oxygen concentration seem to be equivalent mechanisms for introducing these holes.

The drop in T_N, however, is so sensitive to oxygen content that the current literature is unclear about the value of y which produces the maximum T_N in La_2CuO_{4+y}. The idea that magnetic frustration is caused by electron holes introduced by excess oxygen[11] suggests that La_2CuO_4 is intrinsically antiferromagnetic with the maximum T_N occurring for stoichiometric La_2CuO_4. However, due to the difficulty of preparing sufficiently homogeneous and stoichiometric samples and due to the uncertainties in absolute determinations of oxygen content, the stoichiometry of La_2CuO_4 with the highest T_N has not been verified. Johnston *et al.*[17] carrying out thermogravimetric measurements, believed accurate to $\Delta y \approx 0.01$, found that their samples with $200 < T_N < 300$ K were oxygen deficient, with $y \approx -0.035$. They interpret this apparent discrepancy with theory as indicating the presence of a slight La deficiency in their samples. The two possible forms of the phase diagram based on their results are given in Fig. 1.

In this paper we present evidence that the phase boundary shown in the right portion of Fig. 1 is correct, i.e., that stoichiometric La_2CuO_4 has the highest T_N. Our evidence is based on perturbed $\gamma\gamma$ angular correlations (PAC) experiments with ^{111}In-^{111}Cd, a probe known for high sensitivity at extreme dilution. This makes it sensitive to lattice defects,[18] static magnetic order,[19] and magnetic spin fluctuations[20] in a wide variety of systems.

Our PAC experiments on La_2CuO_{4+y} were performed at Clark University, and are focused on samples which show susceptibility maxima at $T_N = 317(3)$ K, the highest value so far published. The samples were doped with ≤ 10 ppm of radioactive ^{111}In, and permit observation of a combined magnetic-dipole–electric-quadrupole interaction produced by the crystal field and the magnetic ordering of the sample. Analysis of the observed precession leads to a temperature dependence of the electric-field-gradient (EFG) asymmetry, $\eta(T)$, and the magnetic hyperfine field, $B_{hf}(T)$, and provides strong evidence that the ^{111}In/^{111}Cd probe resides at the La site. Analysis of

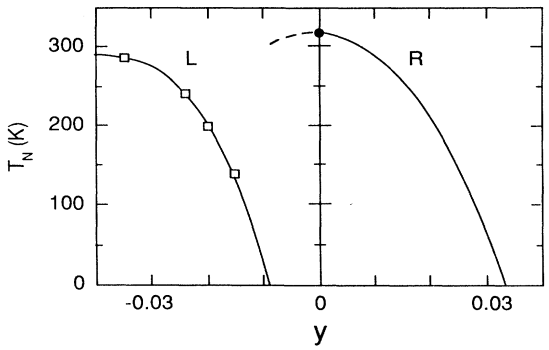

FIG. 1. Two possible forms of the magnetic phase diagram of La_2CuO_{4+y} illustrate the significance of the 1–2 % uncertainty inherent in all bulk determinations of La_2CuO_4 stoichiometry. The left curve, L, which is based on thermogravimetric analysis as described in Ref. 17, shows a *decrease* in T_N with *increasing* oxygen content starting at an apparent maximum at $y=-0.035$. The right curve, R, assumes the same relative behavior as L, but with the maximum in T_N located at $y=0.000(16)$ as proposed in the present paper, and independently by Aharony in Ref. 11. In this context it is important to note that the apparent discrepancy between the L and R curves dissolves if one assumes a 1% compensating La deficiency in the L sample.

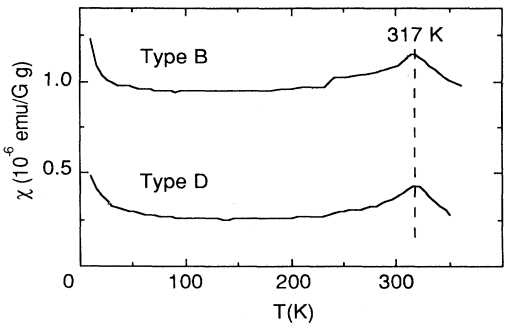

FIG. 2. Susceptibility as a function of temperature for "minimum-vacuum-annealed" (type B) and "hard-vacuum-annealed" (type D) samples. The peaks at 317(3) K agree within error with the PAC result of $T_N=314(4)$ K obtained for type B sample, as shown in Fig. 7.

$B_{hf}(T)$ yields $T_N=314(4)$ K, in agreement with susceptibility peaks in the same samples. The observed temperature dependence of $\eta(T)$ is consistent with the orthorhombic distortion, including a transition to the tetragonal phase at $T_0\sim 540$ K.

As discussed here, the ^{111}In-^{111}Cd probe also provides a new approach for locating the zero in y for La_2CuO_{4+y}. This is based on analysis of the PAC Fourier linewidth, which demonstrates that the probe environment is essentially defect free, i.e., stoichiometric. In this context it is essential to understand that in reaching this conclusion we *do not* require a quantitative understanding of the magnitude of the EFG. Rather, our argument depends on interpretation of the experimentally observed linewidth.

II. SAMPLES AND APPARATUS

Starting materials were of two kinds: (1) a 10×2-mm^2 disk, having 66% of the theoretical density, made at the University of Connecticut and (2) a $2\times 5\times 10$-mm^3 rhomboid of similar density, made at AT&T Bell Laboratories. Via x-ray diffraction both showed the nominal crystallographic structure of La_2CuO_4.[1,21] Most of our measurements were made with a piece of the material used in earlier muon-spin-rotation work by Budnick *et al.*[22] Our 50–100-mg PAC samples were prepared by depositing ~ 10 μCi of carrier-free 2.8-d ^{111}In dissolved in neutralized 0.05 M HCl solution, followed by a two-stage heat treatment.

(1) To diffuse the activity and provide a common starting point for subsequent annealing, all samples were heated in flowing O_2 including: (a) 1 h each at 773, 873, 973, 1073, and 1173 K; (b) 9 h at 1273 K; (c) 13 h cooling at ~ 25 K/h to 773 K; and (d) O_2 and oven shutoff followed by natural cooling.

(2) To adjust their O content, the samples were further prepared in four ways: Type A: "oxygenated sources," were stored in air, but received no further heat treatment. Type B: "minimal-vacuum-anneal sources," were vacuum heated in 10^{-6} torr to 1083 K, followed immediately by vacuum cooling over ~ 13 h to 773 K, at which point the oven was turned off, and samples were naturally cooled for 4 h. Type C: "intermediate-vacuum-annealed sources," were made as in type B, but with 0.5–3 h at 1083 K before start of cooling. Type D: "hard-vacuum-annealed sources," were made as in type B, but with 6–9 h at 1083 K.

Samples for which the radioactivity had decayed were analyzed via the superconducting quantum interference device (SQUID) magnetometer at the National Magnet Lab (MIT), yielding well-defined susceptibility peaks, as illustrated in Fig. 2. These indicate that both type B and D samples have distinctive peaks at 317(3) K, which we interpret as measures of T_N independent of the PAC results given below. Except for the fact that all published values of T_N are significantly lower, our susceptibility data are similar to those of others.[13,23–26]

For PAC measurements we used a standard slow-fast coincidence system with four BaF_2 detectors gated on the 171–245 keV $\gamma\gamma$ cascade of ^{111}Cd, the daughter of ^{111}In. Four coincidence spectra, two each at counter angles 90° and 180°, were combined to obtain the perturbation function, $G_2(t)$. Spectrometer details and data reduction methods have been described elsewhere.[27,28]

III. ANALYSIS OF PAC SIGNALS WELL ABOVE T_N

PAC results for the range $337\le T\le 351$ K, well above T_N, are illustrated in Figs. 3 and 4 in terms of Fourier transforms and time domain data. All time spectra have an unanalyzed, highly inhomogeneous anisotropy component in the first 15 ns, which occurs with varying intensity in different samples, but does not vary with annealing of a given sample and shows no temperature dependence.

This makes K-capture aftereffects implausible, but strongly suggests that some ^{111}In atoms are trapped in grain boundaries or other large defects. We do not consider the inhomogeneous component further, and focus on signals with well-defined frequencies which we identify with the crystalline material.

The remainder of our time spectra consist of distinctive precessional components that we have analyzed via a quadrupole frequency,

$$\omega_Q=(\pi/20)eQV_{zz}/h \ ,$$

and an asymmetry parameter

$$\eta\equiv(V_{xx}-V_{yy})/V_{zz} \ ,$$

where $Q=+0.83(13)$ b is the nuclear electric-quadrupole moment of the 245 keV state[29] and V_{ii} are the principal components of the diagonalized electric-field gradient (EFG). Where f is the fraction of ^{111}In atoms occupying a given site, each spectrum was fitted to one or more terms of the form

$$G_2(t)=(f/5)\{1+\tfrac{13}{7}\cos\omega_0 t+\tfrac{10}{7}\cos[(2-\xi)\omega_0 t] +\tfrac{5}{7}\cos[(3-\xi)\omega_0 t]\} \quad (1)$$

with f, ω_0, and ξ free. Derivable from well-known analytic solutions for the m-state energy levels,[30] ω_0 and ξ are related to ω_Q and η by expressions

$$\omega_0=2\alpha\omega_Q\sqrt{3}\sin(\tfrac{1}{3}\arccos\beta) \ , \quad (2a)$$

$$\xi=\tfrac{5}{2}-(\sqrt{3}/2)\cot(\tfrac{1}{3}\arccos\beta) \ , \quad (2b)$$

where

$$\beta=80(1-\eta^2)/\alpha^3, \quad \alpha=[28(1+\eta^2/3)]^{1/2} \ . \quad (2c)$$

Four distinctive precessional signals are found for the four annealing procedures described: type A, a single, damped signal with an EFG characterized at 351 K by $\eta^A=0.71(1)$ and $\omega_Q^A=49.3(4)$ Mrad/s; type B, a single, undamped signal with a nearly axially symmetric EFG, characterized at $T=344$ K by $\eta^B\approx0.118(4)$ and $\omega_Q^B\approx70.1(2)$ Mrad/s; type C, a linear combination of two signals consisting of type B (above) and type D (below); and type D, a slightly damped signal with a single nearly axially symmetric EFG, characterized at 337.8 K by $\eta^D\approx0.114(4)$ and $\omega_Q^D\approx80.3(1)$ Mrad/s.

The spectra indicate a continuous transformation of

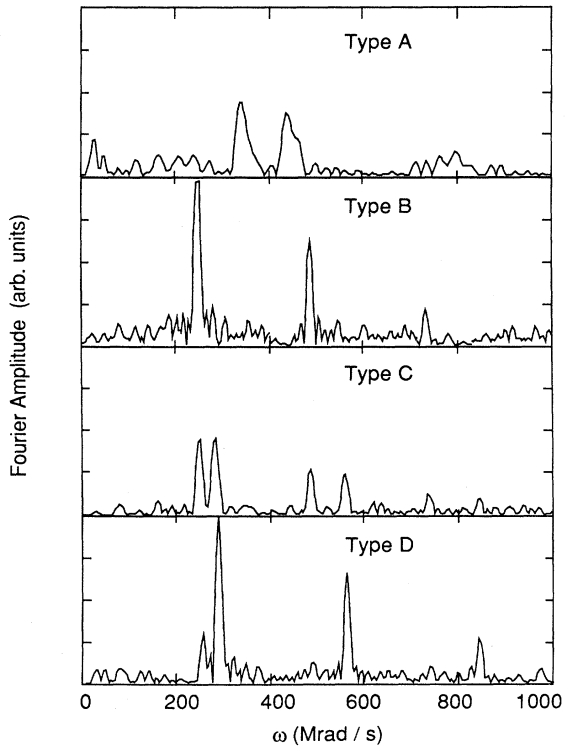

FIG. 3. Fourier transforms of PAC spectra near 340 K for four types of sources. These spectra demonstrate the sensitivity of the signals to the annealing procedure: type A—"oxygen annealed"; type B—"minimal vacuum annealed"; type C—"intermediate vacuum annealed"; type D—"hard vacuum annealed." For further definition of these terms, see the text.

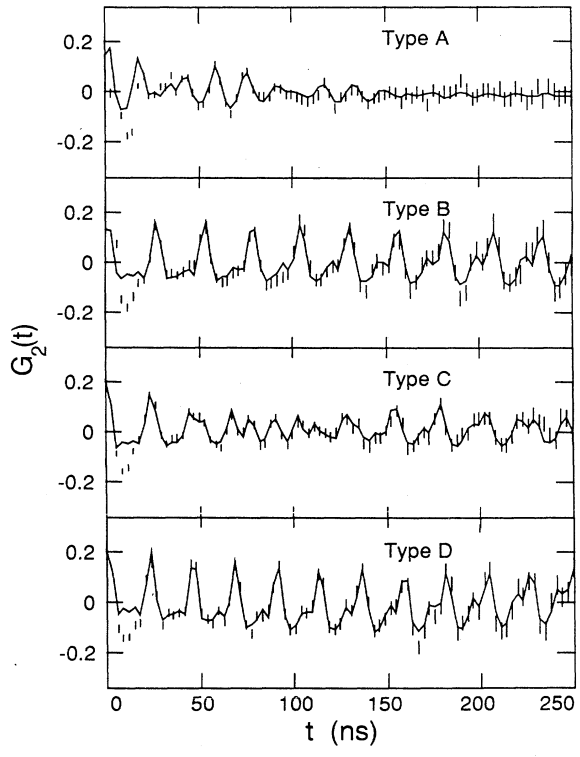

FIG. 4. Time domain PAC spectra corresponding to the Fourier transforms in Fig. 3. The data are fit with a static electric-quadrupole interaction as defined in Eqs. (1) and (2) of the text. For clarity of graphical presentation the measured spectra have been summed eight channels at a time. The amplitude of $G_2(t)$ has been normalized to unity for the effective anisotropy (including angular attenuation) expected for the 171–245 keV cascade of ^{111}Cd.

the *vacuum annealed* samples from type *B* to *D*, with *C* exhibiting a mixed phase. Type *A*, the *oxygenated* sample, shows a Meissner fraction at 4.2 K and showed no magnetic order down to 77 K. Of the four types, *B* is unique in its absence of damping. In the rest of this paper we do not consider *A* further, and focus instead on *B* and *D*.

IV. ANALYSIS OF PAC SIGNALS NEAR AND BELOW T_N

A. Minimum vacuum anneals (type *B*)

As T is lowered from 344 K towards T_N, *B* spectra retain a constant site fraction and an essentially *undamped* signal, while showing a small, continuous change in η, as given in Table I. Between 319.8 and 312.6 K the Fourier lines corresponding to ω_0 and $(3-\xi)\omega_0$ split into doublets, whereas the line corresponding to $(2-\xi)\omega_0$ remains unsplit (Fig. 5).

It can be seen from the energy levels for nuclear spin $I=\frac{5}{2}$ calculated by Matthias, Schneider, and Steffen[31] that such behavior is expected for a particular form of combined electric-quadrupole–magnetic-dipole interaction. Where $\mu=-0.766(3)$, μ_N is the nuclear magnetic moment of the 245 keV state,[32] this form is described by a Larmor frequency, $\omega_L \equiv 2\pi\mu B_{\rm hf}/hI$, with $\omega_L/\omega_Q \ll 1$ and $B_{\rm hf}$ at a polar angle $\theta \simeq \pi/2$ with respect to the z axis of the diagonalized EFG's principal axis system. In treating this interaction quantitatively we approximated the effect of η and ω_L as independent, small perturbations of the dominant quadrupole interaction, but did not consider the interaction of $B_{\rm hf}$ and the EFG asymmetry, and therefore have no information about the azimuthal angle, ϕ, locating $B_{\rm hf}$ in the xy plane. Leaving ω_0, ξ, ω_L, and θ free, the time spectra were fitted as illustrated in Fig. 6, indicating that the data are well accounted for. Numerical results are given in Table I, and details of the analysis in the Appendix.

The remarkable aspect of the data below T_N is that, like those above T_N they are free of detectable additional lines as well as damping of the principal line. To interpret this result we make use of two experimental effects found in a wide variety of systems:[18,33,34] (1) nearest-neighbor charge defects produce quadrupole frequency shifts in the range of 50–250 Mrad/s, including type *D* samples of La_2CuO_4 (see following), and (2) a random distribution of more distant charge defects produces line broadening in the range of $\Delta\omega_0 \sim 5$–25 Mrad/s.

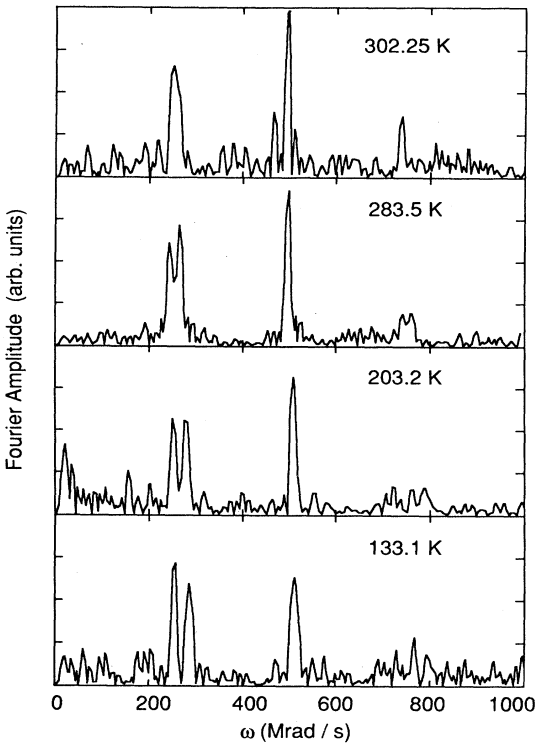

FIG. 5. Fourier transforms of type *B* samples below T_N. These indicate magnetic order with $B_{\rm hf}$ nearly perpendicular to V_{zz}. This is concluded from the splitting of the Fourier lines with frequency of ω_0 and $(3-\xi)\omega_0$, but not $(2-\xi)\omega_0$, as described in the text.

Combining the absence of additional lines and proposition (1) implies for type *B* that we have no evidence for nearest-neighbor charge defects. (Not ruled out, though unlikely, is the possibility of a unique, locally trapped charge defect.) Proposition (2) and the absence of experi-

TABLE I. Fitted parameters for type *B* samples.

Γ (K)	ω_0 (Mrad/s)	ξ	ω_Q (Mrad/s)	η	ω_L (Mrad/s)	θ (deg)
344	246.5(5)	0.035(3)	70.1(2)	0.118(4)		
319.8	247.8(5)	0.046(3)	70.1(3)	0.136(4)		
312.6	248.4(9)	0.048(7)	20.2(3)	0.138(10)	1.8(1.1)	
302.25	248.2(7)	0.050(5)	70.1(3)	0.141(8)	4.5(0.2)	78.8(1.6)
283.5	248.1(8)	0.050(2)	70.1(1)	0.141(3)	5.9(0.1)	78.7(0.4)
274.6	249.3(4)	0.058(3)	70.2(2)	0.158(4)	6.2(0.2)	77.6(0.3)
250	248.2(9)	Fixed			6.7(0.7)	
240	249.6(7)	0.071(5)	70.0(2)	0.170(6)	8.0(0.4)	78.8(0.8)
220	252.5(5)	0.078(4)	70.5(2)	0.178(5)	7.8(0.3)	80.0(1.0)
203.2	252.1(4)	0.081(3)	70.3(2)	0.182(4)	8.3(0.2)	76.1(0.4)
133.1	256.8(5)	0.100(4)	70.9(3)	0.200(4)	9.6(0.3)	76.0(0.3)

mental line broadening at a level of $\Delta\omega_0/\omega_0 < 0.02$ permits placing a limit on the more distant defect concentration. Assuming that these more distant charge defects reside in shells 2 and 3 beyond the nearest-neighbor shell, we are dealing with a population of 45 oxygen sites at an average distance of 5.5 Å. If a 20% population of probe atoms with at least one distant defect produces detectable line broadening, this implies a Poisson distribution of distant defects having a concentration equivalent to

$$x_d \leq 0.20/45 \sim 0.4 \text{ at. } \% \ .$$

Thus, without detailed knowledge of possible charge defect distributions this leads to the estimate that $|y| \leq 0.016$. This result establishes the zero point in y to an accuracy equivalent to the best chemical analysis.[35] The argument is not specific to the oxygen defects but can, in fact, be applied to the sum of all charge defects.

1. The magnetization curve

With D, T_N, and β free, a three-parameter power-law fit to the reduced field

$$B_{\rm hf}(T)/B_{\rm hf}(0) = D(1 - T/T_N)^{\beta} \tag{3}$$

yields $D = 1.15(20)$, $T_N = 314(4)$ K, and $\beta = 0.27(6)$ for

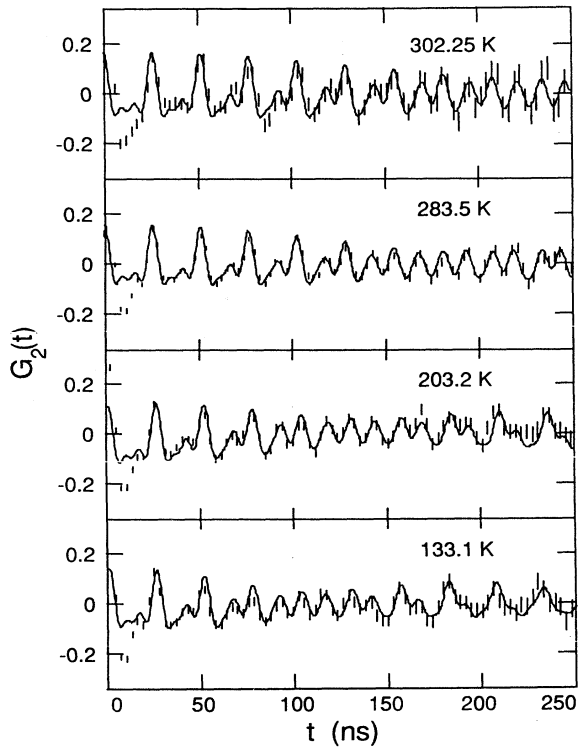

FIG. 6. Time domain spectra of type B sources below T_N. The magnetic component is indicated by the periodic modulation, $\pm 3/2\omega_L$, of the dominant quadrupole frequency, ω_0. Because of the constraints imposed by the nuclear halflife, $\tau_{1/2} = 85$ ns, and the ratio $\omega_L/\omega_0 \ll 1$, at most one period of the beat pattern is visible.

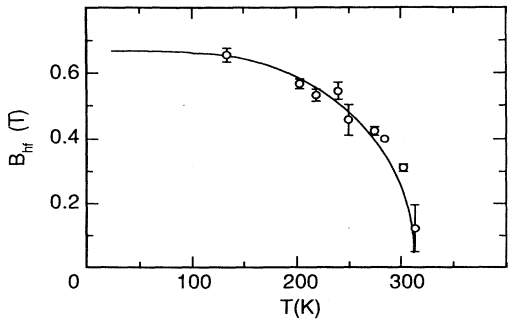

FIG. 7. Temperature dependence of the magnetic hyperfine field $B_{\rm hf}(T)$ for type B samples. The curve represents a molecular field calculation for spin $S = \frac{1}{2}$, a saturation field $B_{\rm hf}(0) = 0.66$ T, and a Néel temperature of $T_N = 314$ K.

$1 - T/T_N < 0.1$. Whereas the value of β is insufficiently asymptotic for a test of critical phenomena theory,[36,37] the value for T_N is in good agreement with the susceptibility data of Fig. 2. The behavior of $B_{\rm hf}(T)$ for $T \leq 314$ K can be approximated via a spin $S = \frac{1}{2}$ molecular field model, as shown in Fig. 7, indicating that data reflect expected bulk magnetization behavior observed previously via muon spin rotation[22] and neutron scattering.[7]

The saturation field of $B_{\rm hf}(0) = 0.66(4)$ T is too small for ^{111}Cd in the Cu site. This follows from typical values of the supertransferred field, $B_{\rm hf}(0) \approx 20$ T, for ^{111}In-^{111}Cd in octahedrally coordinated magnetic oxides[38] and the corresponding expectation of $B_{\rm hf}(0) \approx 12$ T for ^{111}In-^{111}Cd in the square planar Cu site in La_2CuO_4. If our probe substitutes for the La, on the other hand, $B_{\rm hf}(0) \approx 0.7$ T is reasonable, and quite consistent with $B_{\rm hf}(0) \approx 0.1$ T observed via ^{139}La nuclear quadrupole resonance (NQR).[39-41]

2. Temperature dependence of the EFG

Examination of Table I shows that $\omega_Q(T)$ is essentially independent of T, whereas $\eta(T)$ increases as $T \to 0$. Assuming that the temperature variation of η is a consequence of the orthorhombic distortion of the sample, we fixed the orthorhombic to tetragonal transition at $T_0 = 538$ K, as deduced from the linear relation between T_0 and T_N (Ref. 17) and fit our asymmetry parameter to

$$\eta(T) = \eta(0)(1 - T/T_0)^{\Phi} \tag{4}$$

with $\eta(0)$ and Φ free, and obtained $\eta(0) = 0.25(1)$ and $\Phi = 0.74(3)$, as illustrated in Fig. 8. Our result for the exponent agrees strikingly with $\Phi = 0.744$ deduced by Vaknin[42] for crystallographically defined asymmetry parameter,

$$\eta'(T) \equiv 2(c - a)/(c + a) \ ,$$

of the rectangular lattice of the CuO_2 planes. Because both Cu and La suffer similar orthorhombic distortions of the EFG principal axes, the observed behavior of $\eta(T)$ cannot be used to decide whether the ^{111}In is in the Cu or La site.

The result $\eta(0) = 0.25$ differs by a factor of ~ 10 from

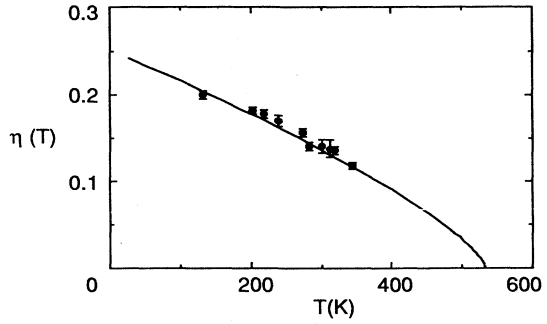

FIG. 8. Temperature dependence of the EFG asymmetry parameter $\eta(T)$ for type B sources. The curve is a power-law fit to Eq. (4) with $\eta(T)$ and Φ free and the tetragonal-orthorhombic transition fixed at $T_0=538$ K, as described in the text.

the values $\eta=0.02$ $\eta=0.03$ seen for ^{139}La NQR (Ref. 39) and ^{63,65}Cu NMR (Ref. 43), respectively. The observed difference is not regarded as significant since $\eta\equiv(V_{xx}-V_{yy})/V_{zz}$ is sensitively dependent on the local structure of the quadrupole coupling for different probes.

3. *The angle between B_{hf} and V_{zz}*

Finally, our analysis yields a fitted value of $\theta=77(3)°$ for the polar angle between $B_{\rm hf}$ and V_{zz}, a result closely comparable to either $\theta=78.7(3)°$ found via ^{139}La NQR (Ref. 39) and $\theta=79°$ found via ^{63,65}Cu NMR (Ref. 43). Though our measured value of θ strongly suggests that the ^{111}In is in either the Cu or La site, it also cannot be used to distinguish between them.

B. Hard-vacuum anneals (type *D*)

As $T\rightarrow T_N^+$, type D spectra, like type B, retain a constant site fraction and exhibit the same smooth $\eta(T)$, with $\eta^D\approx\eta^B=0.12$ near $T=317$ K. There are, however, two important differences with respect to type B: (1) The quadrupole interaction is distinctly higher, with $\omega_Q^D/\omega_Q{}^B\approx1.14$; (2) whereas type B is strictly static and homogeneous, all type D spectra show some damping, and cannot be reliably fit below T_N.

For $317\leq T\leq340$ K we fit type D spectra to a form similar to Eq. (1), but with the addition of three independent damping constants τ_1, τ_2, and τ_3. Our fitting equation was therefore

$$G_2(t)=(f/5)\{1+\tfrac{13}{7}\exp(-t/\tau_1)\cos(\omega_0 t)+\tfrac{10}{7}\exp(-t/\tau_2)\cos[(2-\xi)\omega_0 t]+\tfrac{5}{7}\exp(-t/\tau_3)\cos[(3-\xi)\omega_0 t]\} \quad (5)$$

with results above T_N given in Table II.

Because of the similarity of η for types B and D, and the fact that type D is obtained from type B with additional vacuum annealing, we propose that the ^{111}In has not moved, but acquired a nearest-neighbor O vacancy. This appears particularly plausible because we are able to *reverse* the $B\rightarrow D$ transformation by reannealing in oxygen. If the vacancy lies along the orthorhombic b axis we expect no significant change in η, in agreement with our finding $\eta^D\approx\eta^B=0.12$.

The proposed nearest-neighbor O-vacancy state cannot be related to a bulk oxygen deficiency of the crystal because T_N for type D and B do not differ significantly. Rather, the vacancy must be a *local property* connected with vacancy trapping by the extremely dilute (≤10 ppm) ^{111}In probe, as observed, for example, for a variety of ^{111}In-vacancy interactions in metals.[18,33]

Above 322 K the damping times τ_1, τ_2, and τ_3 are approximately in the ratio $1:\frac{1}{2}:\frac{1}{3}$, as expected for a small static quadrupole inhomogeneity with $\Delta\omega_0\approx5$ Mrad/s. By analog to metals[18,33] this can be attributed to defects beyond the nearest neighbor of the ^{111}In probe. Below 322 K the damping increases sharply as $T\rightarrow T_N^+$, and is reminiscent of critical spin dynamics[26] and/or a distribution of T_N. We cannot distinguish between these possibilities, nor can we fit the spectra below $T=317$ K.

V. SUMMARY AND CONCLUSION

A. Bulk behavior of type *B*

We interpret type B samples, representing "minimal vacuum anneals," as reflecting the bulk properties of the sample. This is based on three separate propositions: (1) The T_N, as determined via the susceptibility, peak agrees with the PAC value of T_N to within error. (2) The behavior of $B_{\rm hf}(T)$ follows a molecular field model. (3) The behavior of $\eta(T)$ reflects the crystallographic character of the known orthorhombic distortion.

B. Stoichiometric character of type *B*.

We argue that type B samples are close to stoichiometric, as indicated by undetectable damping of

TABLE II. Fitted parameters for type D samples.

T (K)	ω_0 (Mrad/s)	ξ	ω_Q (Mrad/s)	η	τ_1 (ns)	τ_2/τ_1	τ_3/τ_1
337.8	282.1(3)	0.033(3)	80.3(1)	0.114(4)	1700(700)	0.55(45)	0.21(19)
328.0	283.2(4)	0.035(5)	80.3(2)	0.118(5)	720(130)	0.53(16)	0.26(10)
322.2	283.0(4)	0.029(3)	80.7(2)	0.108(5)	900(200)	0.31(14)	0.50(32)
319.9	283.7(5)	0.035(3)	80.7(2)	0.118(5)	820(350)	0.76(36)	0.36(21)
318.2	285.1(8)	0.043(5)	80.8(2)	0.130(4)	340(120)	1.5(6)	0.28(14)
317.1	284.0(8)	0.034(6)	80.8(3)	0.116(10)	220(50)	1.8(6)	0.45(20)

the PAC spectrum. Through comparison of the line broadening to that observed in defect studies in other materials, we conclude that $|y| \leq 0.016$.

C. Local vacancy trapping in type *D*

We interpret type *D*, representing the "hard-vacuum annealed sources," as indicating both nearest-neighbor and distant defects. Because type *D* does not involve a change in T_N, the nearest-neighbor defect *cannot* reflect the bulk O content, but must involve vacancy trapping by the ^{111}In probe.

D. Site assignment

Whereas experimental results for $\eta(T)$ and θ are consistent with the ^{111}In-^{111}Cd in either the Cu or La site, the observed value of $B_{\rm hf}(T)$ is consistent only with the La site. We therefore conclude that our probe atoms reside in the La site.

The most significant result of our work is the conclusion that stoichiometric La_2CuO_4 has the highest T_N. We believe this constrains theoretical models of La_2CuO_4 and its role in superconductivity. In particular, our picture of the maximum in the magnetic phase diagram favors the theoretical assumptions proposed by Aharony.[11]

In addition, our PAC experiments appear to have a significant advantage over conventional chemical analysis: through linewidth analysis as presented in this paper, they provide an absolute calibration for the zero of defect concentration. To take advantage of this, experiments are currently underway to map the entire magnetic phase diagram via observed broadening of the PAC spectrum.

ACKNOWLEDGMENTS

The suggestion that type-*B* samples involve a combined interaction was first made by A. Kleinhammes. Many useful comments were received from group member N. Rosov throughout the course of the work. For additional samples of La_2CuO_4 we thank M. Eibschütz of AT&T Bell Laboratories. Experimental assistance in the early stages was received from group members P. Lidbjörk, A. Kleinhammes, and R. Schuhmann. Some aspects of the PAC fitting programs are due to G. S. Collins of Washington State University, and others to F. Pleiter of the Rijksuniversiteit, Groningen, The Netherlands. Use of the MIT SQUID is gratefully acknowledged. Research support was received under National Science Foundation (NSF) Grant Nos. DMR 83-03611 and DMR 87-23033.

APPENDIX

For any homogeneous and static hyperfine interaction the perturbation function $G_2(t)$ is a discrete sum of components[44]

$$G_2(t)=\sum_k s_k \cos(\nu_k \omega_Q t) , \tag{A1}$$

where ν_k reflects the energy differences and s_k the transition probabilities between nuclear m states. For a combined electric-quadrupole–magnetic-dipole interaction, s_k and ν_k depend on $Y=\omega_L/\omega_Q, \eta$, and angles θ and ϕ which describe the orientation of the magnetic field relative to the principal axes of the EFG tensor.

In our treatment of $^{111}CdLa_2CuO_4$ PAC, we simplified the fitting procedure by deriving polynomial expressions which approximate s_k and ν_k to 0.1% over the range of observed interactions, i.e., $0 \leq \cos\theta \leq 0.2$, and $0 \leq Y \leq 0.3$. In deriving the expressions we further simplified our analysis by a two step procedure, as follows.

(1) For $\eta=0$, tabulated values of $\nu_k(\cos\theta, Y)$ and $s_k(\cos\theta, Y)$ were fit with polynomials of the form

$$\nu_k(\cos\theta, Y)=a_{0k}+(a_{1k}+b_{1k}\cos\theta)Y + (a_{2k}+b_{2k}\cos\theta)Y^2 \tag{A2}$$

and

$$s_k(\cos\theta, Y)=c_{0k}+c_{1k}Y+c_{2k}\cos\theta . \tag{A3}$$

The initial values for ν_k and s_k were generated by a program written by Pleiter[45] which, for arbitrary Y and θ, numerically diagonalizes the combined interaction Hamiltonian and translates the eigenvalues and eigenvectors into PAC frequencies and amplitudes.

(2) The case $\eta \neq 0$ was incorporated into the model for $G_2(t)$ by shifting the frequency of each Zeeman doublet by the same amount ξ [Eq. (2b)] as the equivalent quadrupole line would have been shifted if it were not split by the magnetic interaction. This yields the final form

$$G_2(t)=\sum_k s_k(\theta, Y, 0)\cos\{[\nu_k(\theta, Y)-\xi_k(\eta)]\omega_Q\} . \tag{A4}$$

Since our analysis did not incorporate the interaction of the hyperfine field and the small EFG asymmetry, our expressions do not depend on ϕ, the orientation of the magnetic field in the xy plane.

[1] R. J. Birgeneau and G. Shirane, in *Physical Properties of High Temperature Superconductors,* edited by D. M. Ginsberg (World Scientific, Singapore, 1989), pp. 151–211.

[2] R. J. Birgeneau, R. A. Cowley, G. Shirane, J. A. Tarvin, and H. Guggenheim, Phys. Rev. B **21**, 317 (1980).

[3] R. A. Cowley, R. J. Birgeneau, G. Shirane, H. J. Guggenheim, and H. Ikeda, Phys. Rev. B **21**, 4038 (1980).

[4] J. W. Essam, in *Phase Transitions and Critical Phenomena,* edited by C. Domb and M. S. Green (Academic, New York, 1972), Vol. 2, pp. 197–270.

[5] S. Kirkpatrick, Rev. Mod. Phys. **45**, 574 (1973).

[6] T. Freltoft, J. E. Fischer, G. Shirane, D. E. Moncton, S. K. Sinha, D. Vaknin, J. P. Remeika, A. S. Cooper, and D. Harshman, Phys. Rev. B **36**, 826 (1987).

[7] K. Yamada, E. Kudo, Y. Endoh, Y. Hidaka, M. Oda, M. Suzuki, and T. Murakami, Solid State Commun. **64**, 753

(1987).
[8]J. I. Budnick, B. Chamberland, D. P. Yang, Ch. Niedermayer, A. Golnik, E. Recknagel, M. Rossmanith, and A. Weidinger, Europhys. Lett. **5**, 651 (1988).
[9]D. R. Harshman, G. Aeppli, G. P. Espinosa, A. S. Cooper, J. P. Remeika, E. J. Ansaldo, T. M. Riseman, D. Ll. Williams, D. R. Noakes, B. Ellman, and T. F. Rosenbaum, Phys. Rev. B **38**, 852 (1988).
[10]V. J. Emery and G. Reiter, Phys. Rev. B **38**, 4547 (1988).
[11]A. Aharony, R. J. Birgneneau, A. Coniglio, M. A. Kastner, and H. E. Stanley, Phys. Rev. Lett. **60**, 1330 (1988).
[12]R. J. Birgeneau, M. A. Kastner, and A. Aharony, Z. Phys. B **71**, 57 (1988).
[13]D. C. Johnston, J. P. Stokes, D. P. Goshorn, and J. T. Lewandowski, Phys. Rev. B **36**, 4007 (1987).
[14]R. M. Fleming, B. Batlogg, R. J. Cava, and E. A. Reitman, Phys. Rev. B **35**, 7191 (1987).
[15]P. M. Grant, S. S. P. Parkin, V. Y. Lee, E. M. Engler, M. L. Ramirez, J. E. Vazquez, G. Lim, R. D. Jacowitz, and R. L. Greene, Phys. Rev. Lett. **58**, 2482 (1987).
[16]Y. Kitaoka, K. Ishida, K. Amaya, and K. Asayama, Physica C **153-155**, 733 (1988).
[17]D. C. Johnston, S. K. Shinha, A. J. Jacobson, and J. M. Newsam, Physica C **153-155**, 572 (1988).
[18]F. Pleiter and C. Hohenemser, Phys. Rev. B **25**, 106 (1982).
[19]C. Hohensemser, T. Kachnowski, and T. K. Bergstresser, Phys. Rev. B **13**, 3154 (1976).
[20]C. Hohenemser, L. Chow, and R. M. Suter, Phys. Rev. B **26**, 5056 (1982).
[21]K. Yamada, E. Kudo, Y. Endoh, K. Tsuda, M. Tanaka, K. Kokusho, H. Asano, F. Izumi, M. Oda, Y. Hidaka, M. Suzuki, and T. Murakami, Jpn. J. Appl. Phys. **27**, 1132 (1988).
[22]J. I. Budnick, A. Golnik, Ch. Niedermayer, E. Recknagel, M. Rossmanith, A. Weidinger, B. Chamberland, M. Filipkowski, and D. P. Yang, Phys. Lett. A **124**, 103 (1987).
[23]T. Fujita, Y. Aoki, Y. Yoshiteru, Y. Maeno, J. Sakurai, H. Fukuba, and H. Fuji, Jpn. J. Appl. Phys. **26**, L368 (1987).
[24]T. Thio, T. R. Thurston, and N. W. Preyer, P. J. Picone, M. A. Kastner, H. P. Jenssen, D. R. Gabbe, C. Y. Chen, R. J. Birgeneau, and A. Aharony, Phys. Rev. B **38**, 905 (1988).
[25]R. L. Greene, H. Maletta, T. S. Plaskett, J. G. Bednorz, and K. A. Muller, Solid State Commun. **63**, 379 (1987).
[26]H. Ishii, H. Sato, N. Kanazawa, H. Takagi, S. Uchida, K. Kitazawa, K. Kishio, K. Fueki, and S. Tanaka, Physica B **148**, 419 (1987).
[27]A. R. Arends, C. Hohenemser, F. Pleiter, H. de Waard, L. Chow, and R. M. Suter, Hyperfine Interact. **8**, 191 (1980).
[28]C. Hohenemser and R. B. Schuhmann, Hyperfine Interact. **30**, 109 (1986).
[29]P. Herzog, K. Freitag, M. Reuschenbach, and H. Valitzki, Z. Phys. A **294**, 13 (1980).
[30]E. Gerdau, J. Wolf, H. Winkler, and J. Brausfurth, Proc. R. Soc. London Ser. A **311**, 197 (1969).
[31]E. Matthias, W. Schneider, and R. M. Steffen, Phys. Rev. **125**, 261 (1962).
[32]H. Bertschat, H. Haas, F. Pleiter, E. Recknagel, E. Schlodder, and B. Spellmeyer, Z. Phys. **270**, 203 (1974).
[33]A. R. Arends, and F. Pleiter, Hyperfine Interact. **12**, 143 (1982).
[34]W. Bolse, M. Uhrmacher, and K. P. Lieb, Phys. Rev. B **36**, 1818 (1987).
[35]J. D. Jorgensen, B. Dabrowski, S. Pei, D. G. Hinks, L. Soderholm, B. Morosin, J. E. Schirber, E. L. Venturini, and D. S. Ginley, Phys. Rev. B **38**, 11337 (1988).
[36]R. M. Suter and C. Hohenemser, J. Appl. Phys. **50**, 1814 (1979).
[37]C. Hohenemser, N. Rosov, and A. Kleinhammes, Hyperfine Interac. **49**, 267 (1989).
[38]H. H. Rinneberg and D. A. Shirley, Phys. Rev. B **13**, 2138 (1976).
[39]H. Lütgemeier and M. W. Pieper, Solid State Commun. **64**, 267 (1987).
[40]I. Furo and A. Janossy, Jpn. J. Appl. Phys. **26**, 1307 (1987).
[41]Y. Kitaoka, S. Hiramatsu, K. Ishida, T. Kohara, and K. Asayama, J. Phys. Soc. Jpn. **56**, 3024 (1987).
[42]D. Vaknin, S. K. Sinha, D. E. Moncton, D. C. Johnston, J. M. Newson, C. R. Safinya, and H. E. King, Jr., Phys. Rev. Lett. **58**, 2802 (1987).
[43]T. Tsuda, T. Shimizu, H. Yasuoka, K. Kishio, and K. Kitazawa, J. Phys. Soc. Jpn. **57**, 2908 (1988).
[44]R. M. Steffen and H. Frauenfelder, in *Perturbed Angular Correlations,* edited by E. Karlsson, E. Matthias, and K. Siegbahn (North-Holland, Amsterdam, 1964), pp. 1–90.
[45]F. Pleiter (private communication).